Applied Catalysis B: Environmental 244 (2019) 414–426

Contents lists available at ScienceDirect

Applied Catalysis B: Environmental

journal homepage: www.elsevier.com/locate/apcatb

Effect of Mn on Co/HMS-Mn and Co/SiO_2-Mn catalysts for the Fischer-Tropsch reaction

Héctor G. Salazar-Contreras[a], Angel Martínez-Hernández[a,*], Alicia A. Boix[b], Gustavo A. Fuentes[c], Enelio Torres-García[d]

[a] Universidad Autónoma de Nuevo León, UANL, Facultad de Ciencias Químicas, Av. Universidad S/N, San Nicolás de los Garza, Ciudad Universitaria, C.P. 66451, N.L, Mexico
[b] Instituto de Investigaciones en Catálisis y Petroquímica, INCAPE (FIQ, UNL-CONICET), 3000, Santa Fe, Argentina
[c] Universidad Autónoma Metropolitana-Iztapalapa, Área de Ingeniería Química, A.P. 55-534, 09340, México, D.F, Mexico
[d] Biomass Conversion Management, Instituto Mexicano del Petróleo, Eje Central Lázaro Cárdenas Norte 152, C.P. 07730, México City, Mexico

ARTICLE INFO

Keywords:
Fischer-Tropsch
Cobalt
Manganese
SiO_2
HMS

ABSTRACT

The structural changes of cobalt deposited on SiO_2 and Hexagonal Mesoporous Silica (HMS) supports were studied when Mn was used as a promoter and added to the catalyst during the synthesis of the supports by the sol-gel method. This synthetic method was used to promote the contact between the highly dispersed Mn in the supports and the Co added by incipient impregnation. The characterization results reveal that the presence of Mn promoted the dispersion of deposited cobalt oxide particles, causing a "wetting-like" effect of the cobalt oxide on the support surface, which led to a decrease of the average particle size of cobalt oxide from 13 to 10 nm in absence and presence of Mn respectively. The characterization results indicate that the Co^{2+} species react with Mn ions to form a likely Mn-Co spinel. Additionally, it was found that the promotion effects of Mn on the catalytic activity at atmospheric pressure for the Fischer-Tropsch synthetic reaction on both studied supports were significantly different because of the low metal loading used (< 5 wt% of Co and 0.8 wt% of Mn) and the differences in their specific surface areas and texture. In the case of the catalysts using SiO_2 as the support, the addition of Mn resulted in an enhancement of the CO consumption, whereas for the case of catalysts with HMS as the support, its presence was counterproductive, possibly because there was limited contact between the Mn and Co and because a fraction of the Mn was incorporated into the HMS framework. Furthermore, the catalytic tests at high pressure (20 bar) indicates that the catalysts were not fully selective toward hydrocarbon production, indicating that there are secondary reactions (e.g., water gas-shift reaction) due to non-reduced Co-oxide species. Additionally, at these operating conditions, the CO consumption rate increased proportionally as function of the Mn loading in the catalysts, whereas the selectivity toward olefins declined.

1. Introduction

The consumption of fossil fuels (mainly gasoline, diesel and aircraft fuel) by the transportation sector has led to a high demand of oil, which increases the cost of extraction due to the depletion of the oil fields located in accessible areas and deep water exploitation regions. The high demand for anthropogenic processes will cause a decreasing availability of this non-renewable resource worldwide in the future. In fact, shale oil and gas have attracted great attention because the technology to recover them has been enhanced. Additionally, there are a number of important reserves and the level of production has increased [1]. However, these are still non-renewable resources that will eventually decline and disappear. In addition, the severe problems of pollution caused by the combustion of fossil fuels around the world have prompted the search for more environmentally friendly alternatives.

The search for alternatives to fossil fuels, e.g., biofuels, has acquired an immediate and future significance because this could contribute to the depletion of greenhouse gases due to the use of renewable sources inside the carbon cycle. An example of these could be the biological treatment of organic wastes (municipal waters, food residuals, etc.) [2]. Currently, one of the main alternatives for the production of liquid fuels from non-fossil sources are the GTL (gas to liquid) or BTL (biomass to liquid) processes, which consist of the formation of synthesis gas (a mixture of CO and H_2) and its subsequent feeding into the reactor where the Fischer-Tropsch synthesis reaction (FTS) occurs on a solid

* Corresponding author.
E-mail address: angel.martinezhn@uanl.edu.mx (A. Martínez-Hernández).

https://doi.org/10.1016/j.apcatb.2018.11.067
Received 29 July 2018; Received in revised form 16 November 2018; Accepted 22 November 2018
Available online 23 November 2018
0926-3373/

catalyst, resulting in a mixture of hydrocarbons (synthetic oil) that can be separated into different products [3]. Currently, small scale BTL processes using municipal wastes are already commercially available.

Furthermore, the FTS reaction could be performed with catalysts based on Ru, Fe or Co as the active metal. The catalysts prepared from Ru have high activity toward long-chain hydrocarbons. However, Ru is a scarce element in the earth and therefore quite expensive, which inhibits its use in an industrial scale [4,5]. Recently, it has been reported that a hybrid catalyst using Ru as a promoter has shown good activity and selectivity for the FTS reaction, which opens the possibility for its use in commercial facilities [6,7]. Furthermore, Fe-based catalysts are used commercially due to the low cost of Fe (compared with the other metals), high selectivity to olefins, and high activity toward the water gas shift (WGS) reaction, which is needed when the synthesis gas contains a low H_2 concentration [4,8]. On the other hand, it has been reported that Co-based catalysts have a higher yield and selectivity towards linear paraffinic hydrocarbons compared with Fe-based catalysts, showing low selectivity for the WGS reaction, and they are not inhibited by the water formed as by-product of the FTS reaction [8,9]. It is has been proposed that mesoporous supports are convenient for the synthesis of catalysts used in the FTS reaction. For example, the materials MCM-41 (Mobil Composition of Matter), SBA-15 (Santa Barbara Acids) and HMS (Hexagonal Mesoporous Silica) have been used in several studies to perform the FTS reaction. The MCM-41 consists of an amorphous-silicate framework that forms hexagonal pores with specific surface areas up to 1200 m^2/g, large pore volume with a narrow pore size (1.5 and 20 nm) distribution. The thin pore walls are the cause of low chemical and hydrothermal stabilities of this material. In the case of SBA-15, the pore walls are between 3–6 nm that confer to this material a high thermal stability compared with other mesoporous materials (e.g. MCM-41 and HMS), with a combined micro- and mesoporosity and pore size in the range of 0.5–3 nm and 4–14 nm (uniform mesoporosity) respectively [10]. On the other hand, the HMS material has a wormhole-like pore structure, with a thick pore wall between 0.9–3 nm, and a pore diameter size between 2.2–4.4 nm [11,12]. In addition, it has found that this material has a better mechanical stability than the above mentioned materials because the lattice of HMS has certain flexibility [13], presumably because the mesopores are shorter in this material.

Among the catalyst supports that have been studied for the FTS reaction, hexagonal mesoporous silica (HMS) and SiO_2 have shown interesting results. It has been reported for the former that its pore size has a restrictive effect for the formation of high molecular weight compounds (waxes). For example, Lira et al. [14] compared the performance of Co supported on HMS and SiO_2 for the FTS reaction at 20 bar and 230 °C. They found that the HMS support favored the production of hydrocarbon components in the ranges of gasoline (C_5-C_9) and diesel (C_{10}-C_{15}), whereas the amorphous SiO_2 support showed a trend towards the formation of higher molecular weight hydrocarbons (C_{19+}). They suggested that the mass transport of reactants and products into the HMS limits the chain growth, forming less heavy hydrocarbons (wax). Bragança et al. [15] conducted several catalytic tests using bimetallic catalysts of Co and Fe supported on HMS and SBA-15, and from their results, it was suggested that the catalysts using HMS as a support showed higher selectivity to C_{5+} because there was a greater dispersion of metallic cobalt (active sites) on the surface, in addition to the easiest access of reactants to these sites.

The addition of promoters to the catalysts is a key factor in order to attain the maximum activity, selectivity and stability because the dispersion of active sites and the redox properties can be modified, causing an enhancement in the catalytic activity and selectivity toward the desired FTS reaction products as a result. Among the studied promoters, the Mn promotion of Co-based catalyst has been related with the stronger adsorption of CO on the Co active sites [16], resulting in a higher chain growth of hydrocarbons. In separate studies, Yin et al. [17] and Martínez et al. [18] associated the presence of Mn (2 wt%) in Co/HMS (15 wt% of Co) and Co/SBA-15 (20 wt% of Co) catalysts, respectively, with a higher segregation of active Co° particles. Nevertheless, both authors reported that the presence of Mn resulted in a low conversion of CO and also in a lower selectivity towards C_{5+} compounds.

To avoid the effect of the different particle size of cobalt active sites on the FTS reaction, Feltes et al. [19] synthetized catalysts where the Co° particle size was almost the same (they used the strong electrostatic adsorption method) regardless of the amount of Mn added to the Mn/Co/TiO_2 catalysts (10 wt% of Co). They suggested that the addition of small amounts of Mn (0.03 wt%) promoted the stabilization of Co particles in a completely reduced state, facilitating the formation of smaller particles over the TiO_2 support. This dispersion of Co particles prevented the cobalt ripening and enhanced the catalytic activity. However, they also found that the use of higher Mn loadings could block the active sites, resulting in less reducibility of the active metal and therefore lower catalytic activity. The same effect of the Mn loading has been observed by several authors, and the beneficial Mn promotion for the FTS reaction has been assigned either to a weakening of the atomic cobalt-silicon interaction, an increase in the amount of Co-MnO interfaces, a Lewis acid site formed between the interaction of Co and Mn (where Mn promotes changes in the electron density of the Co° phase), or a higher stabilization of the CO adsorbed on the active sites [20–25].

It has been reported also that the interaction between the Co and Mn results in the formation of a stable Co-Mn spinel [26], which hinders the reduction of the Co spinel during the reduction process. The similar effect has been reported for Fe-based catalysts where the formation of an stable Fe-Mn spinel is formed resulting in a higher activity and stability of the catalyst against the deactivation [27–30], these effects are attributed to the formation of the Fe carbide during the exposition of the catalysts to the synthesis gas [31–33]

Thus, the association between Co° active sites and Mn when the latter is present in low contents has resulted in a better catalytic performance. However, the comprehension regarding the promotion effect of Mn on the Co° active sites is not fully understood. Usually, the Mn is loaded after the Co impregnation, which can lead to the coverage of cobalt active sites, which makes the observation of Co-Mn interactions difficult with large Mn contents. The aim of this work is to evaluate the influence of Mn as promoter when it is incorporated during the synthesis of the SiO_2 and HMS supports in order to investigate the effect of Mn-Co interactions on the FTS reaction.

2. Experimental

2.1. Catalyst synthesis

The HMS supports using the method described by Tanev and Pinnavaia were synthesized [34]. Briefly, the synthesis consisted of dissolving dodecylamine ($C_{12}H_{25}NH_3$, Sigma Aldrich) as a surfactant in ethanol following the addition of water (ethanol/water = 0.3 v/v) under vigorous stirring until a homogeneous mixture was obtained. The desired amount of manganese precursor ($Mn(NO_3)_2{\cdot}4H_2O$, Sigma Aldrich) was dissolved in a tetra-ethyl ortho-silicate ($SiO_4(C_2H_5)_4$, Sigma-Aldrich) solution under vigorous stirring and aggregated in the template solution. The nominal content of Mn in the supports was varied from 0 to 0.8 wt% so the Mn/Co ratio ranged from 0 to 0.19. The SiO_2 was synthesized with the same procedure described above; however, in this case, a higher ethanol/water ratio was used (8.5 v/v). In both cases, the obtained gel was filtered and dried at room temperature for 24 h and subsequently calcined at 640 °C in static air. The supports were labeled HMS-*x* and SiO_2-*x*, where *x* represents the weight percent of Mn. The catalysts by the incipient wetness impregnation method were synthesized using a solution of cobalt nitrate ($Co(NO_3)_2{\cdot}6H_2O$, Sigma Aldrich). The impregnated supports were dried at 80 °C for 2 h and subsequently calcined at 550 °C for 4 h in static air. Table 1 summarizes the contents of Mn and Co measured by Atomic Absorption

Table 1
Chemical composition of Co/HMS-*x* and Co/SiO_2-*x* catalysts, with *x* = wt% of Mn.

Sample	Co (wt%)	Mn (wt%)	Mn/Co ratio (Mole/Mole)
Co/HMS	4.1	0.0	0.00
Co/HMS-0.2	4.4	0.2	0.04
Co/HMS-0.4	4.3	0.4	0.10
Co/HMS-0.8	4.2	0.8	0.19
Co/SiO_2	4.5	0.0	0.00
Co/SiO_2-0.2	4.2	0.2	0.05
Co/SiO_2-0.4	4.7	0.4	0.08
Co/SiO_2-0.7	4.8	0.7	0.15

Spectrometry (AAS) (220FS SpectrAA, Varian) for the synthesized catalysts. For the reaction tests at high pressure, the catalysts were prepared as follows: the support powders were pressed in a stainless steel die using 7 tonnes/in^2. The resulting tablet was crushed and sieved to obtain particles of size between 100–120 mesh. The particles were mechanically stabilized by adding 12.5 wt.% of colloidal silica as a binder (Bindzil® 50/80, kindly donated by AKZO NOBEL). The mechanically stabilized particles were dried at 80 °C and calcined afterwards at 500 °C. Finally, the Co was deposited following the same procedure as the catalysts powders.

For all of the catalysts, the Co loading was almost the same in order to directly compare the differences in the catalytic activity due to the Mn/Co ratio, whereas the low content of Co (~ 4.5 wt%, see Table 1) was chosen in order to facilitate the observation of Co-Mn interactions, trying to minimize the possible masking effects of bulk cobalt oxide in the characterization of the catalysts.

2.2. Catalyst characterization

The textural properties of the supports and catalysts were measured with N_2 physisorption (ASAP 2020, Micromeritics). The surface areas were evaluated by using the BET method, and the pore size distributions were determined by the BJH method. The low and wide angle X-ray diffraction patterns were measured with a Siemens D500 diffractometer by using CuK_α radiation (λ = 1.54 Å) from 0.55° to 7° and 10° to 70°, respectively, in order to observe the ordered structures of the HMS supports and crystalline phases of the catalysts, respectively. Raman spectroscopy (Thermo Scientific DXR Raman Microscope with a 532 nm laser) and UV–vis-NIR spectroscopy (Cary 5000 Series, Varian) equipped with a diffuse reflectance accessory (Praying Mantis, Harrick) were used to identify the differences in the cobalt oxide caused by the presence of Mn. The catalysts were also characterized with the temperature-programmed reduction technique (TPR) in homemade equipment for evidence as to the effect of Mn on the reducibility of cobalt oxide. This was conducted by using 30 mg of catalyst while a gas stream of 20 cm^3/min composed of 5% H_2 in an argon balance flowed through the reactor. The experiments in the following sequence were performed: i) in a 1 st stage the reactor temperature was raised from room temperature to 500 °C with a heating ramp of 10 °C. Then the temperature was kept by 2 h, and thereafter the reactor was allowed to cool at 300 °C; ii) in a 2nd stage the temperature of the reactor was raised from 300 °C to 900 °C using the same heating ramp than in the 1 st stage.

X-ray photoelectron spectroscopy (XPS) characterization was performed in a multi-technique system (SPECS) equipped with a dual Mg/Al X-ray source and hemispherical PHOIBOS 150 analyzer operating in the fixed analyzer transmission (FAT) mode. The spectra were obtained with pass energy of 30 eV, with the Al-Kα X-ray source (hγ = 1486.6 eV) at 200 W. The pressure in the chamber was less than 2.0×10^{-9} mbar. The calcined catalysts were degassed in a vacuum at 300 °C (10^{-3} mbar) and then reduced in situ with a gas mixture composed of 5% H_2/Ar at 400 °C for 15 min. Spectral regions corresponding to Co 2p, Mn 2p, O 1 s, Si 2 s, C 1 s and Si 2p core levels were recorded for each sample, and the binding energy (BE) of Si 2p = 103.5 eV was considered as an internal reference. The data treatment was performed with the CasaXPS Software [35]. The peak areas were determined by integration employing a Shirley-type background. Peaks were considered to be a mixture of Gaussian and Lorentzian functions in a 70/30 ratio.

2.3. Catalytic reactions

The FTS reaction at atmospheric pressure and 220 °C was carried out in a tubular quartz reactor (φ = 10 mm), and 20 bar at 240 °C in a stainless steel reactor (φ = 16 mm). In the case of atmospheric pressure, the reactor was loaded with 100 mg of catalyst. The gas stream consisted of a mixture of H_2/CO/N_2 (20/10/5 cm^3/min), with a total flow of 35 cm^3/min. The apparent densities of Co/HMS-x and Co/SiO_2-x catalysts were 0.15 and 0.27 g/cm^3, respectively, so the synthesized SiO_2 support was used to compensate for the changes in the catalyst bed volume in order to keep the same space velocity in the reactor (21 nL / h *g_{cat}) for all of the catalytic tests. For the high pressure reaction tests, the reactor was loaded with 250 mg of catalyst and the differences in the catalytic bed were compensated using SiC (Strem Chemicals) with particle size of 100 mesh; the gas stream consisted of a mixture of H_2/CO/Ar (25/25/50 cm^3/min), with a total flow of 100 cm^3/min; in this conditions the space velocity was 24 nL / h *g_{cat}. The pressure in the reactor was automatically controlled with a backpressure regulator attached to a stepper motor, and the motor was controlled via a desktop computer. On the other hand, it was not possible to control the temperature inside of the catalytic bed by instability of the temperature control. Instead the reactor temperature was controlled by the temperature of the electric furnace, while the temperature of the bed was recorded during the whole reaction test. For the catalytic test, the reaction stream was flowed through the reactor at 230 °C, this condition was kept by 6 h, and afterwards the temperature was raised to 240 °C with a heating ramp of 0.5 °C/min. In this case, it was used the Ar as internal reference in order to measure the CO consumption.

In both cases, the reactor effluent with non-condensed compounds (gas phase) was analyzed online by a gas chromatograph (GC6820, Agilent) equipped with thermal conductivity (TCD) and flame ionization (FID) detectors. Prior to the FTS reaction, the catalysts were reduced in situ at 500 °C for 2 h and 7 h, while 20 and 45 cm^3/min of a gas mixture containing 10% v/v of H_2 and N_2 as the balance flowed through the reactor in the case of the catalysts in powder and pelletized respectively. The identification and quantification of the main reaction products was performed by comparing the GC retention times with those obtained with paraffin and olefin hydrocarbon standards (C_1-C_6, Aldrich). In the high pressure tests, the reactor effluent passed through a stainless steel cold trap placed at the reactor outlet where the condensable products, e.g., the water and heavier hydrocarbons (C_{6+}) were trapped. The collected oil was characterized offline by gas chromatography; however the other potential products (e.g., oxygenated compounds and CO_2) could not be measured due to experimental restrictions. In the case of reaction tests at atmospheric pressure, the reported conversion was taken once the measured CO concentration in the reactor effluent reached a constant value; in this case, this occurred after 10 h since the beginning of catalytic tests. The following calculations were based in the work of Dinse et al. [22]. For the reaction at atmospheric pressure the CO consumption rate was calculated using Eq. (1), and the selectivity of the catalyst was calculated with Eq. (2).

$$COconsumptionrate = \frac{n_{CO}^{inlet} X_{CO}^{1}}{w_{Co}^{Red}};\text{with}\quad X_{CO}^{1} = \frac{\sum_{1=1}^{n} \nu_i C_i}{C_{CO}^{0}} \tag{1}$$

$$Hydrocarbonselectivity^{1} = \frac{\nu_i n_i}{n_{CO}^{inlet} * X_{CO}^{1}} \tag{2}$$

In the case of the catalytic tests at 20 bar the CO consumption rate

was calculated using Eq. (3), and the selectivity of the catalyst was calculated with Eq. (4).

$$COconsumptionrate = \frac{n_{CO}^{R-fed} X_{CO}^{20}}{w_{Co}^{Red}}; \text{with} \quad X_{CO}^{20} = \frac{n_{CO}^{R-feed} - n_{CO}^{R-out}}{n_{CO}^{R-feed}} * 100 \tag{3}$$

$$Hydrocarbonselectivity^{20} = \frac{Q_{TOS}^{out} \sum_{i=1}^{n} \nu_i C_i}{n_{TOS}^{fed} * X_{CO}^{20}} \tag{4}$$

where n_{CO}^{inlet} is the molar flow at the reactor inlet, X_{CO}^{1} is the CO conversion at atmospheric pressure, w_{Co}^{Red} is the weight of Co° obtained in the catalyst activation, C_{CO}^{0} is the concentration of CO at the reactor inlet, ν_i is the stoichiometric coefficient, n_i is the moles of the i-th hydrocarbon formed during the reaction, C_i is the concentration of compound i-th, n_{CO}^{R-fed} is the total moles of CO fed during the time on stream (TOS) catalytic test, X_{CO}^{20} is the CO conversion at 20 bar, n_{CO}^{R-feed} and n_{CO}^{R-out} are the CO moles at the reactor inlet and outlet respectively calculated using Ar as the internal standard, and Q_{TOS}^{out} is the volumetric flow at the reactor outlet during the TOS test. The olefin/paraffin ratio was calculated in both cases using the Eq. (5).

$$O/P = \frac{n_{C_2H_4} + n_{C_3H_6} + n_{C_4H_8}}{n_{C_2H_6} + n_{C_3H_8} + n_{C_4H_{10}}} \tag{5}$$

3. Results and discussion

3.1. Textural characterization

The N_2 adsorption-desorption isotherms for the HMS-*x* supports (Fig. 1, curves a–d) showed the type IV (IUPAC) characteristic of mesoporous solids [12,36]. The sharp increase in the adsorbed volume of N_2 at low relative pressure (P/Po < 0.1) is in agreement with solids that have a high specific surface area. Additionally, the four solids also showed the so-called framework-confined mesoporosity [34] between 0.3 < P/Po < 0.5, which corresponds to the volume of N_2 occupied by the ordered structure of the HMS-*x*, indicating a unimodal pore size. The adsorption-desorption isotherms for the Co/HMS-*x* catalysts (Fig. 1, curves e–h) showed that the textural characteristics of supports are conserved in their respective catalyst. In Table 2, it can be observed that the pore volume fraction corresponding to the framework-confined mesoporosity (determined using the N_2 adsorption branch between 0.1 < P/P_o < 0.5) is at least half of the total, showing that a unimodal distribution is present even after the calcination of the catalysts. In the cases of SiO_2-*x* supports and Co/SiO_2-*x* catalysts, these showed essentially the same type of N_2 adsorption-desorption isotherms, which correspond to the type II (IUPAC), and this is the reason that only the results for Co/SiO_2-*x* catalysts are shown (Fig. 1, curves i–l). The N_2 adsorption branch for these catalysts showed only a pronounced rise at high relative pressures, which is attributed to the presence of pores with a large size (> 30 nm).

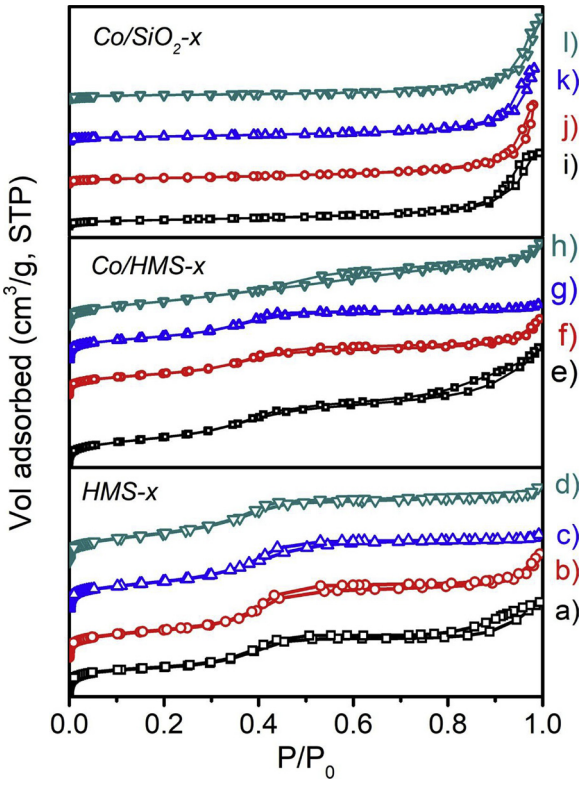

Fig. 1. N_2 adsorption-desorption isotherms of HMS-*x* supports (curves a: x = 0; b: x = 0.2; c: x = 0.4; d: x = 0.8), the Co/HMS-*x* catalysts (curves e: x = 0; f: x = 0.2; g: x = 0.4; h: x = 0.8) and Co/SiO_2-x catalysts (curves i: x = 0; j: x = 0.2; k: x = 0.4; l: x = 0.7). Where x = wt% of Mn.

Table 2
Textural properties obtained from N_2 adsorption-desorption isotherms for supports and Co/HMS-x and Co/SiO_2-x catalysts, where x = wt% of Mn.

Sample	BET surface area (m^2/g)	Average Pore diameter BJH (nm)	Framework confined pore volume (cm^3/g)	Total pore volume (cm^3/g)
HMS	669	3.1	0.6	0.9
HMS-0.2	652	3.1	0.6	1.0
HMS-0.4	650	3.1	0.6	0.7
HMS-0.8	648	2.9	0.6	0.7
SiO_2	437	30	–	1.6
SiO_2-0.4	294	> 30	–	1.7
SiO_2-0.7	234	> 30	–	0.7
Co/HMS	603	3.0	0.5	1.0
Co/HMS-0.2	503	3.0	0.4	0.7
Co/HMS-0.4	504	3.0	0.4	0.5
Co/HMS-0.8	506	3.4	0.4	0.7
Co/SiO_2	297	≥30	–	1.3
Co/SiO_2-0.2	275	> 30	–	1.5
Co/SiO_2-0.4	234	> 30	–	1.4
Co/SiO_2-0.7	199	> 30	–	1.5

For both HMS-*x* and SiO_2-*x* supports, less N_2 adsorption was observed when the Mn content in the solids increased; therefore, the specific surface area decreased according to the increase of the Mn content in the supports (Table 2). Additionally, the textural properties of Co catalysts in Table 2 show that the specific surface areas of both types of catalysts were lower compared with their respective supports, suggesting that a fraction of the Co oxide was inside of the pores or located at the opening of the pore mouth, and in both cases, this restricts the N_2 adsorption.

3.2. Low-angle X-ray diffraction

The low angle XRD patterns for representative HMS-*x* and SiO_2-*x* supports are shown in Fig. 2. As seen that only the HMS-*x* solids showed a single peak at 2θ = 1.8°, which is associated with local hexagonal symmetry (d_{100}) [34]. It can be observed that in the case of the HMS-*x* solids, the peak showed a lower intensity compared with the peak of HMS, indicating that the formation of a wormhole framework structure is lost [12] in this case, which is caused by the presence of Mn ions in the support synthesis. In the inset of Fig. 2, the shift toward a higher 2θ value for the HMS-0.4 support is shown, which is caused by the addition of Mn. This shift indicates that there is a slight increase in the average distance between the pore centers [37]. Due to the synthetic method, it is presumed that Mn is found highly dispersed on the supports and possibly located nearest to structural defects since its presence in the support synthesis hinders the formation of the HMS framework. The fact that supports with Mn have the lowest specific surface area is in agreement with the loss of the framework structure.

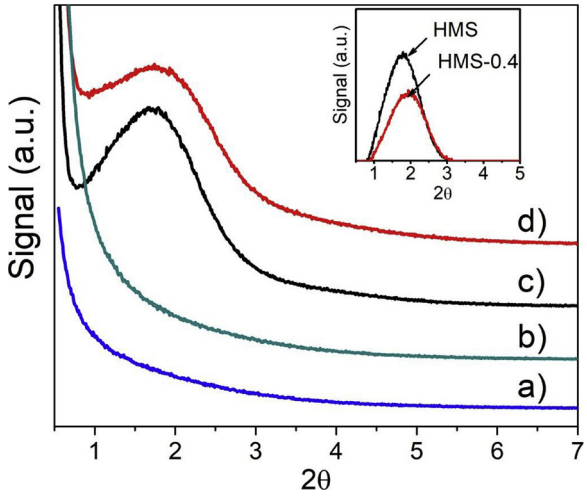

Fig. 2. Low angle XRD for selected HMS-x and SiO_2-x supports, with x = wt% of Mn: SiO_2 a), SiO_2-0.4 b), HMS c), and HMS-0.4 d). The supports were calcined at 640 °C in static air.

3.3. Wide angle X-ray diffraction

The XRD patterns of only calcined catalysts at 550 °C (no peaks attributable to Mn were observed) are shown in Fig. 3. It can be seen that despite the low Co loading, in both types of catalysts, the XRD patterns showed only the representative peaks of Co_3O_4 at 2θ = 31.3°, 36.8°, 44.8°, 59.1° and 65.1°, corresponding to the reflection lines 220, 311, 400, 511 and 440, respectively [38]. The particle size of Co_3O_4 was calculated from the peak at 2θ = 36.8° using the Scherrer equation, and it was found that the particle size ranged from 13 nm in the cases of Co/HMS and Co/SiO_2 and 10 nm for the case of catalysts with the highest Mn content (see Table 3). This result indicates that the presence of Mn caused a decrease in the size of cobalt oxide particles, which is in agreement with the results reported in the literature [22]. Additionally, it has been reported that Co can form solid solutions with Mn [22,24,26,39]; however, due to the low Co loading and the way in which Mn was introduced into the support, it was not possible to distinguish the formation of a mixed oxide or a solid solution between Co and Mn. Furthermore, the main diffraction peak in the XRD patterns (see Fig. 3) does not show a perceptible shift of the main peak. Nevertheless, the formation of a mixed oxide is highly probable in the synthesized catalysts, although this is undetectable by this technique because of the low metal loading used.

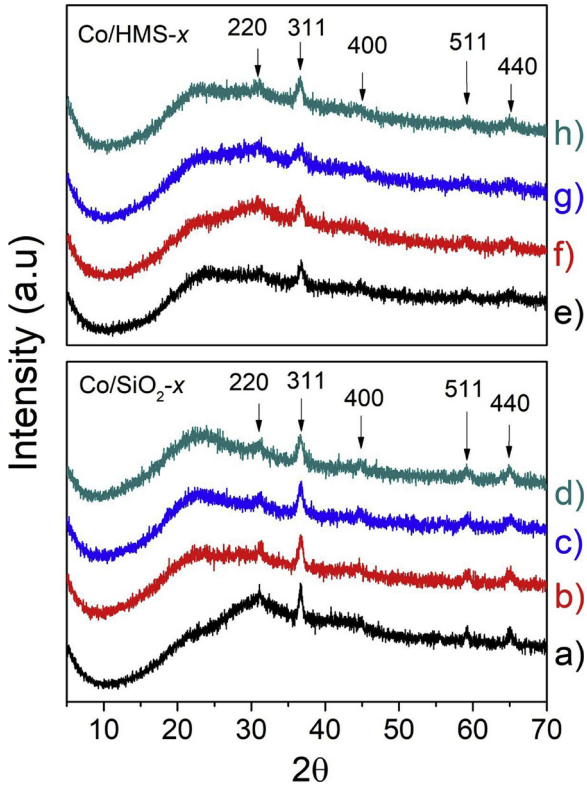

Fig. 3. XRD patterns for only-calcined Co/SiO_2-x and Co/HMS-x catalysts, with x = wt% of Mn: Co/SiO_2 a), Co/SiO_2-0.2 b), Co/SiO_2-0.4 c), Co/SiO_2-0.7 d), Co/HMS e), Co/HMS-0.2 f), Co/HMS-0.4 g), and Co/HMS-0.8 h).

3.4. Temperature programmed reduction (TPR)

The supports characterized by this technique did not display any reduction peak (not shown), even at the highest loading of Mn. However, it is expected that the distribution of the cobalt oxide and therefore the reduction of it on the catalysts will be different because of the presence of Mn in the catalysts. The TPR profiles of the studied catalysts are shown in Figs. 4 and 5.

It has been reported that the reduction of cobalt oxide supported on different silica-based mesoporous materials occurs in two stages. The first stage occurs between 280–350 °C and has been assigned to the reduction of $Co_3O_4 \rightarrow CoO$, while the second stage occurs at 350–420 °C and corresponds to the reduction of $CoO \rightarrow Co^{\circ}$ [40–43]. The reduction profile of the free-Mn catalysts showed essentially two close peaks in the first reduction stage: in the case of Co/HMS these were observed between 250–350 °C and in the case of Co/SiO_2 between 300–420 °C (Figs. 4a and 5 a respectively). In both types of catalysts the presence of Mn resulted in a shift to higher temperature of the second peak which is related with the retarded reduction of $CoO \rightarrow Co0$, coupled with a less consumption of hydrogen, in agreement with an early reduction of Co_3O_4 promoted by the presence of Mn (see UV section). On the other hand, in the second stage of reduction (T > 500 °C) is observed a broad peak between 500–750 °C as the Mn loading increased, which has been related with the reduction of Mn^{4+} and Mn^{3+} to Mn^{2+} [44], or with the reduction of Co species with strong metal-support interactions [14,15,42]. Additionally, in this stage appeared a reduction peak around 820 °C, whose size increased as function of the Mn amount in the supports. The peak is more defined in the case of Co/HMS-x catalysts (Fig. 5); in these there is a high probability that a fraction of the added Mn has been incorporated in the framework of the HMS during the synthesis of the supports, this will be discussed later (see UV–vis section). It has been reported that at 850 °C there is a complete structural collapse of the HMS material [13], therefore the reduction peak observed at 820 °C could be assigned to the reduction of extra-framework Mn (likely from Mn^{3+} to Mn^{2+}) produced by the structural collapse of the HMS.

On the other hand, it has been reported that there is a less reduction degree of Co_3O_4 due to the interaction between Mn and Co. For example, Guse et al. [26] found that the formation of a stable Co-Mn spinel hinders the formation of metallic Co during the reduction process. However, is very difficult to identify the spinel at low Mn loadings, although some authors have been proposed that $Co_{3-x}Mn_xO_4$ spinel is formed (e.g. [22,24,45]). Interestingly, the presence of Mn also hinders the reduction of Fe in the catalysts studied for the FTS reaction, similarly to the effect observed with Co [27–30]. For Fe-based catalysts, it is proposed that the presence of Mn causes the stabilization of the active sites during the FTS reaction, because an iron-carbide species are formed, preventing thus the oxidation of the Fe metallic sites toward the F_3O_4 phase during reaction (e.g. [31–33,46]).

The TPR results suggest that the presence of Mn caused the stabilization against the reduction of Co_xO_y species. This was used as a factor to calculate the degree of reducibility (DR) in order to quantify the effect of the presence of Mn on the reduction of cobalt oxide in the

Table 3
Reducibility for Co supported on HMS-x and SiO_2-x (x = % Mn).

Catalyst	Average Co particle size (nm)[a]	H_2 Consumption (mole) x 10^6		(A1)/(A2) Ratio	Degree of Co reducibility (%)	Total Co reducibility (%)
		1st Reduction stage T ≤ 500 °C (A1)	2nd Reduction stage T > 500 °C (A2)		1st stage (Eq. (6))	A1 + A2
Co/HMS	13	21.4	4.3	5.0	72	86
Co/HMS-0.2	12	18.2	8.7	2.1	60	88
Co/HMS-0.4	10	8.7	11.3	0.8	29	66
Co/HMS-0.8	10	14.6	14.6	1.0	48	96
Co/SiO_2	13	28.5	1.9	15.4	90	96
Co/SiO_2-0.2	13	23.4	3.8	6.2	78	91
Co/SiO_2-0.4	10	23.5	5.6	4.2	70	87
Co/SiO_2-0.7	10	14.2	12.5	1.1	43	80

[a] Calculated with the Scherrer equation from XRD patterns of Fig. 3.

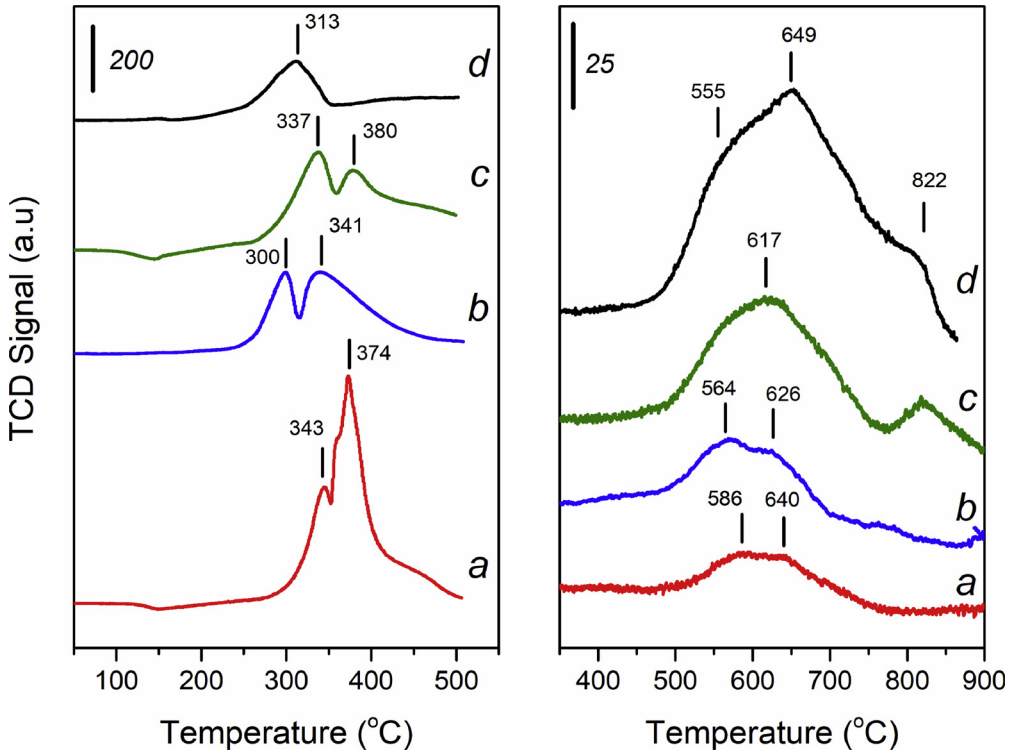

Fig. 4. TPR patterns for Co/SiO_2-x catalysts, with x = wt% of Mn: Co/SiO_2 a), Co/SiO_2-0.2 b), Co/SiO_2-0.4, and Co/SiO_2-0.7 d).

catalysts; this was defined as the ratio between the moles of H_2 consumed during the activation treatment of the catalyst (i.e., the first reduction stage, because only this fraction of reduced Co will be available for the FTS reaction) and the moles of H_2 necessary to reduce all of the Co determined by atomic absorption spectrometry (supposing that it was Co_3O_4), such as is expressed in Eq. (6).

$$DR(\%) = \frac{H_2 consumption in TPR at T \leq 500^oC\,(moles)}{H_2 necesary to reduce total Co_3O_4\,(moles)} \quad (6)$$

The results for both types of catalysts are shown in Table 3. As can be seen, in the Mn-free catalysts, there was not a complete reduction of the cobalt in the first reduction stage, suggesting that some fraction of the deposited Co could be located inside of blocked pores, preventing the contact of the reducible species with the H_2; this could explain why the Co/HMS has a minor reduction degree than the Co/SiO_2 catalyst since the former has a smaller pore size (see Table 2). However, it cannot be discarded the formation of Co silicates by reaction of the CoO produced during the reduction with the silica support [47]. The DR factor decreased for both types of catalysts by the presence of Mn; however it can be observed that the Mn hindered the Co reduction in larger extent in the case of Co/HMS-x catalysts (lower A1/A2 ratios, see Table 3). These indicate that the presence of Mn was detrimental for the reduction of cobalt oxide whatever the Mn loading was. A similar effect of Mn on the reducibility of cobalt oxide has been reported by other authors (e.g., [19,24]). The possible reason that the total reduction of the Co spinel could not be achieved (last column in Table 3) would be the presence of the un-reduced Co-Mn spinel, the formation of Co silicates, or both.

3.5. Raman spectroscopy

In the Raman spectra of the HMS and SiO_2 supports (not showed), the peaks at 485 and 560 cm^{-1} associated with the three and four siloxane rings, a peak at 800 cm^{-1} associated with siloxane linkages (Si-O-Si) and another peak at 965 cm^{-1} associated with Si−OH groups were observed [48–50]. Additionally, a peak at 480 cm^{-1} (small) and another peak at 1100 cm^{-1} were observed in the spectra, and these were assigned to the TEOS [51] that remained in the solid samples after

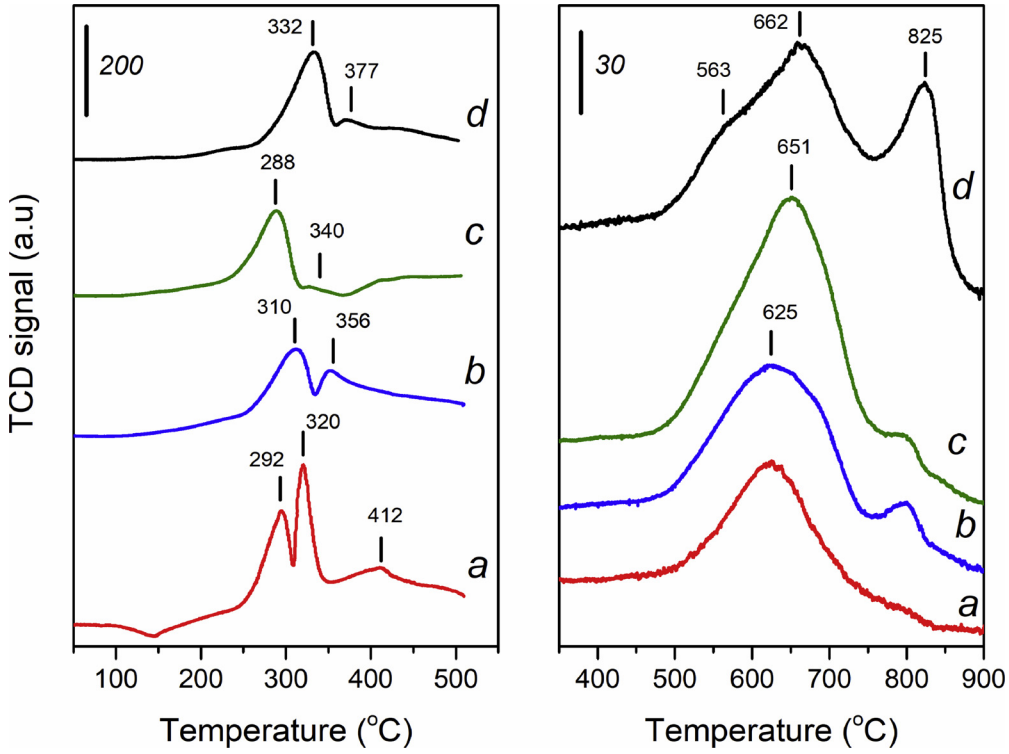

Fig. 5. TPR patterns for Co/HMS-x catalysts, with x = wt% of Mn: Co/HMS a), Co/HMS-0.2 b), Co/HMS-0.4 c), and Co/HMS-0.8 d).

the calcination step.

The spectra obtained for representative catalysts are shown in Fig. 6. Peaks were found at 187, 468, 510, 607 and 674 cm^{-1} that can be assigned to crystalline Co_3O_4 [52–54]. In both types of catalysts, the highest intensity of the peaks was observed for the Co/HMS and Co/SiO_2, whereas when Mn was present, these peaks showed a minor intensity, suggesting a minor amount of Co_3O_4 (or an early reduction caused by Mn). The effect was less evident in the case of Co/HMS-*x* catalysts, probably due to their higher surface areas that prevented greater contact between Co and Mn. It has been reported that the Mn_3O_4 has a characteristic peak at 650 cm^{-1}. The Mn_2O_3 has a peak between 640-650 cm^{-1} and another at 680 cm^{-1}, while a peak at 490 cm^{-1} has been assigned to the asymmetric stretching of bridged oxygen species (Mn−O−Mn) [55,56]. It can be seen from the spectra

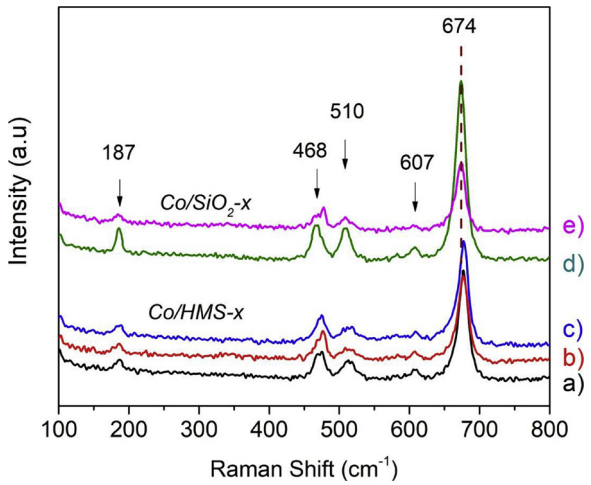

Fig. 6. Raman spectra for representative only-calcined Co/HMS-*x* and Co/SiO_2-*x* catalysts, with x = wt% of Mn: Co/HMS a), Co/HMS-0.2 b), Co/HMS-0.4 c), Co/SiO_2 d), and Co/SiO_2-0.4 e).

(Fig. 6) that none of these peaks for the Co/HMS-*x* and Co/SiO_2-*x* catalysts were observed, probably due to the low Mn content, but this also indicated that the Mn is highly dispersed in the supports.

If the decrease in the intensity of Co_3O_4 peaks was a partial reduction toward CoO, then the characteristic peaks of CoO (455 and 675 cm^{-1}, [53]) could appear. However none of these were observed, likely because the fraction of reduced oxide is small due to the low Co loadings.

3.6. X-ray photoelectron spectroscopy (XPS)

To investigate the chemical state and surface concentration of species in the Co/SiO_2-x catalysts, the photoelectron spectra of samples with different Mn contents were analyzed. This characterization was made only for Co/SiO_2-x catalysts because these were the most active for the FTS reaction (as will be discussed below). From XPS measurements, the binding energies and the full width at half maximum (FWHM) values of the constitutive elements for all of the catalysts were obtained, which were assigned as follows: 532.8 (2.6–2.7) ± 0.1 eV and 154.5 (3.0–3.3) ± 0.1 eV for O 1s and Si 2 s, respectively. The BE of Si 2p at 103.5 eV was considered as an internal reference. Table 4 shows the BEs of Co $2p_{3/2}$ and Mn $2p_{3/2}$ core-levels. Before carrying out the XPS measurements, the samples were degassed in a vacuum at 300 °C (10^{-3} mbar) and then reduced under the flow of a 5% H_2/Ar mixture at 400 °C (at atmospheric pressure).

The spectra of the Co 2p of the Co/SiO_2 catalyst present two components for the Co $2p_{3/2}$ main peak (Table 4), one at 779.9 eV associated with the Co^{2+}/Co^{3+} species of cobalt oxides and the other at a higher BE of 783.0 eV that could correspond to cobalt species that interact with silanol groups [57]. Moreover, the main peak is accompanied by a relatively intense 3d-4 s shake-up satellite peak at 787.2 eV, which is characteristic of Co^{2+} species. Additionally, the cobalt spectra show a spin–orbit splitting of Co $2p_{3/2}$-$2p_{1/2}$ at approximately 15.5 eV. In the reduced catalysts, the concentration of oxidized cobalt species decreases and a new component appears at 777.6 eV, which corresponds to the metal cobalt signal (Fig. 7a). It was found that

Table 4
XPS results for Co/SiO_2-*x* catalysts.

Sample	Binding Energy, eV [c]				(I_{sat}/I_{mp}) [e]	(Mn/Co) [f]
	Mn $2p_{3/2}$	Co $2p_{3/2}$				
		Co- Sil	Co_3O_4	Co°		
Co/SiO_2 [a]	–	783.3	779.9 49% [d]	–	0.45	–
reduced [b]	–	783.0	779.9 41% [d]	777.6 36%	0.38	–
Co/SiO_2-0.2 [a]	641.4 (2.5)	782.5	779.5 62% [d]	–	0.40	0.064 0.051[g]
reduced [b]	640.7 (2.5)	783.1	780.2 35% [d]	777.6 48%	0.35	0.14
Co/SiO_2-0.4 [a]	641.6 (4.7)	783.1	780.0 52% [d]	–	0.31	0.14 0.084[g]
reduced [b]	641.4 (4.8)	782.9	780.4 37% [d]	778.1 33%	0.27	0.22
Co/SiO_2-0.7 [a]	641.4 (4.1)	782.7	780.2 72% [d]		0.48	0.14 0.145[g]
reduced [b]	641.1 (4.0)	782.3	779.6 44% [d]	777.8 10%	0.48	0.15

[a] Calcined catalysts degassed in vacuum at 300 °C (10^{-3}mbar).
[b] *in situ* reduction with 5% H_2/Ar flow at 400 °C.
[c] Binding energy of Si2p = 103.5 eV as internal reference.
[d] Surface concentration of cobalt species.
[e] Intensity ratio, satellite peak/ main peak of Co2p.
[f] Atomic surface ratio from XPS.
[g] Bulk ratio from ICP measurement.

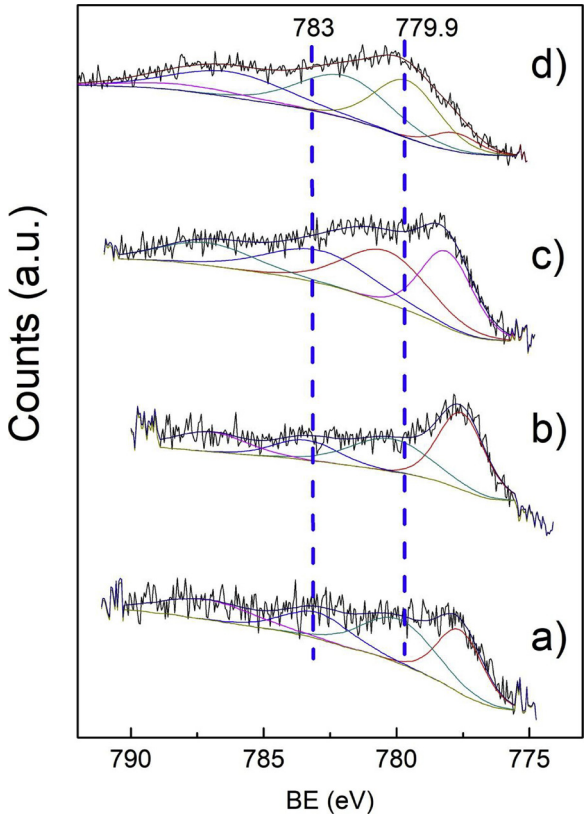

Fig. 7. XPS spectra for reduced Co/SiO_2-x catalysts, with x = wt% of Mn: Co/SiO_2 a), Co/SiO_2-0.2 b), Co/SiO_2-0.4, and Co/SiO_2-0.7 d).

approximately 36% of the total cobalt on the surface is reduced below 400 °C, which is in good agreement with the TPR results (see Section 3.4).

In the case of the only calcined Co/SiO_2-0.2 catalyst (Fig. 7b), the spectrum exhibits two components at 779.5 and 783.1 eV for the Co2$p_{3/2}$ main signal. After reduction, an intense peak at 777.6 eV can be observed, which indicates that 48% of cobalt was completely reduced. Furthermore, a decrease in the I_{sat}/I_{mp} ratio (satellite peak and main peak intensity ratio) suggests that the surface concentration of Co^{2+} species decreases because neither the Co^{3+} of cobalt oxides nor the metallic Co phase present a satellite structure (Table 4).

On the other hand, it was observed that Co/SiO_2-x catalysts show a decrease of cobalt reducibility (below 400 °C) as the Mn content increases, showing lower formation of the metallic cobalt phase, which is in agreement with a decrease of H_2 consumption of the first peak (Table 4). It can be observed that after reduction, the Mn/Co ratio remains constant for Co/SiO_2-0.7 (Fig. 7d), whereas it increases in the cases of Co/SiO_2-0.2 and Co/SiO_2-0.4 catalysts (Fig. 7b and c, respectively). These results suggest that the formation of mixed oxides $CoMnO_x$ is favored as the Mn content increased in the supports because the intimate contact between Co and Mn hindered the reducibility of Co.

The spectra obtained for the Mn 2p region have low intensity and were noisy due that the Mn content in the solids is very low (less than 1%) and is found highly dispersed in the supports. Nevertheless, an analysis considering the SiO_2-0.7 support with the highest Mn content is useful to investigate the possible state of Mn in the supports. The spectrum of the Mn 2p core-level shows a broad peak of Mn 2p3/2 centered at 642.2 eV with a FWHM of 5.3 eV; small changes were observed after in situ reduction at 400 °C, with the BE changing to 642.0 eV and the FWHM = 5.0 eV. Analyzing the corresponding catalysts (Co/SiO_2-0.7), a Mn $2p_{3/2}$ signal at 641.4 eV with a FWHM of 4.1 eV (Table 4) was observed. The BE shift (-0.8 eV) could be associated with the interaction between Co and Mn components. According to the reported data for MnO, Mn_2O_3 and MnO_2 pure oxides, the BE values are approximately 641.2, 641.8 and 642.2 eV, respectively [58,59]. Taking into account the small difference between the reported BE values and the width of the peak, it is possible that oxidized manganese species with oxidation states of (2+) and (3+) coexist, which are interacting with the cobalt oxides and support silica. Finally, the measured surface atomic ratios Mn/Co (Table 4) were close to the bulk values (Table 1), which would indicate that Mn and Co are well dispersed on the surface of the support.

3.7. UV–vis spectroscopy

In Fig. 8, the spectra of SiO_2-*x* and HMS-*x* supports are shown. It can be seen that these show the ligand to metal charge transfer band between 200–300 nm as well as another band centered at 405 and 455 nm for the HMS-x and SiO_2-*x* supports, respectively. The low amount of Mn makes their characterization difficult. However, the band at 405 nm could be assigned to Mn^{2+} in the support framework, such as has been observed in other solids [60], while the band at 455 could be related to Mn^{4+} [61]. For both types of supports, the band between 400–500 nm became broader with the highest Mn loading, which suggests that in these cases, there is a mixing of Mn species (Mn^{2+}/Mn^{4+}). The presence of Mn^{2+} in the supports (mainly in HMS-x) suggests that at low Mn contents, a significant fraction is incorporated into the framework of the support.

The spectra of Co/HMS-0.8 and Co/SiO_2-0.7 catalysts as well as their counterparts without Mn are shown in Fig. 9. These solids were selected because the promoted changes by the presence of Mn are best visualized. It can be seen from Fig. 9 that there are significant differences in the intensity of the cobalt bands due to the presence of Mn, with decreases in the bands observed in both cases. In both types of catalysts, two broad bands are present at 350–600 and 600–800 nm. There are many assignments in the literature for the UV–vis bands of cobalt, presumably due to the diversity of the studied materials and the different phenomena involved in the support-metal interactions. It has been reported that bands at 370–390 and 625–680 nm appear to be

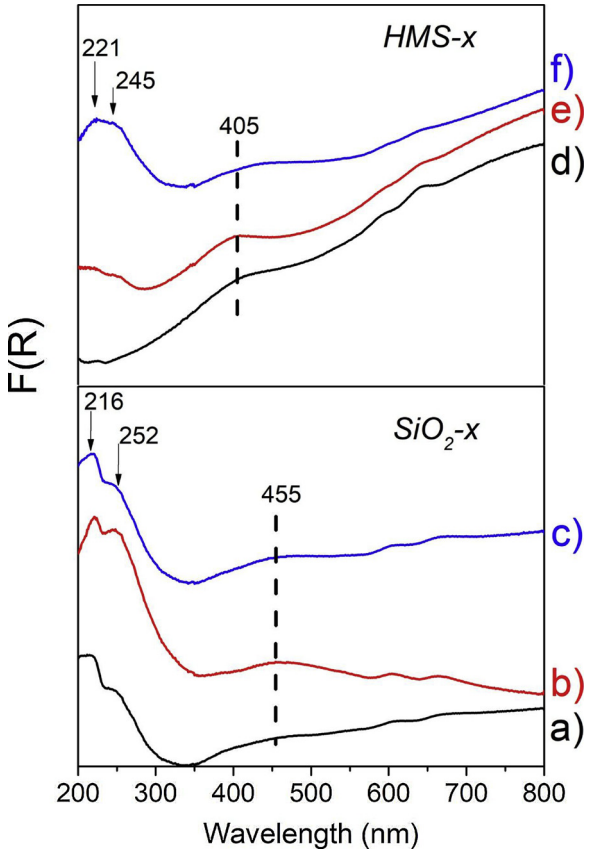

Fig. 8. UV–vis spectra of SiO_2-x and HMS-x supports, with x = wt% of Mn: SiO_2-0.2 a), SiO_2-0.4 b), SiO_2-0.7 c), HMS-0.2 d), HMS-0.4 e), and HMS-0.8 f). The spectra shown were obtained after subtraction of the Mn-free supports.

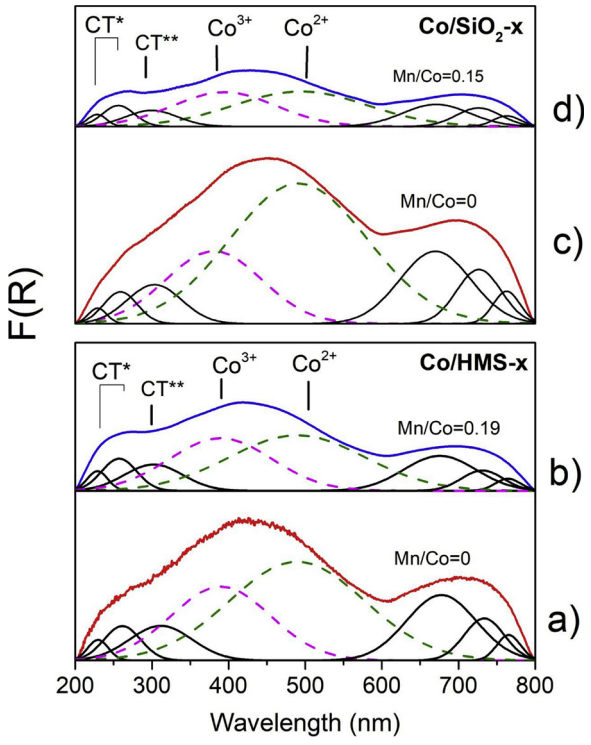

Fig. 9. Deconvolution of UV–vis spectra of only-calcined Co/HMS-x and Co/SiO_2-x catalysts, with x = wt% of Mn: Co/HMS a), Co/HMS-0.4 b), Co/SiO_2 c) and Co/SiO_2-0.7 d).

related with the spinel Co_3O_4 structure [62], which are assigned to cobalt ions in tetrahedral and octahedral coordination, respectively. Additionally, it has been reported that bands at 400 and 700 nm appear as a result of the presence of octahedral Co^{3+} species in Co_3O_4, while octahedral Co^{2+} shows a band at 500 nm [63]. Furthermore, the presence of bands at 340, 410 and 525 nm has been assigned to the charge transfer from $O^{2-} \rightarrow Co^{3+}$, to Co^{3+} in tetrahedral coordination and to Co^{2+} in tetrahedral coordination [64].

Additionally, the band at 250 nm is assigned to the metal-ligand charge transfer $O^{2-} \rightarrow Co^{3+}$ [65] or $O^{2-} \rightarrow Co^{2+}$ [66]. Nevertheless, in this work, it is not possible to infer the particular nature of the bands due to their overlap with the charge transfer band of Mn. From Fig. 9, it can be seen that when the Mn content increases in the catalysts, this becomes more defined because the band centered at 430 nm decreased. This band has been associated in some works with Co^{3+} in octahedral coordination in the Co_3O_4 spinel structure [65,67,68], whereas the centered band at 720 nm has been assigned to Co^{2+} in octahedral coordination [69]. On the other hand, a blueshift in the maximum of the band centered at 562 nm in the case of Co/HMS-0.8 catalysts promoted by the presence of Mn (see Fig. 9) was observed, while for Co/SiO_2-0.7, these maxima do not show an evident shift. To indicate the reason for this shift in the UV–vis region, the spectra were deconvoluted in Gaussian components using eight curves in both cases in order to obtain a good fit of the spectra. From Fig. 9, it can be seen that the most intense bands appear between 380–500 nm, and it is in this region where the main changes are observed. From the literature discussed above, the main bands can be assigned to Co^{3+} (380–400 nm) and Co^{2+} (490–500 nm) in octahedral and tetrahedral coordination, respectively.

Due to the low Mn content in the catalysts, the synthetic method employed for the preparation of supports, and the absence of signals of Mn-oxide in the XRD, TPR and Raman characterizations, a small particle size of Mn oxide is expected (< 10 nm). Thus, when the supports containing Mn are impregnated and thereafter calcined, there is a high possibility that Mn^{4+} is reduced to Mn^{3+} by a thermal effect (oxide decomposition), and in these conditions, it is suggested that the resulting particles have high reactivity due to a lot surface oxygen dangling bonds [70]; thus, the Mn^{3+} could react with the Co atoms formed during the decomposition of the Co-salt, therefore hindering the formation of the Co_3O_4 spinel and forming instead the Mn-Co spinel. It has been reported that above 525 °C, the removal of oxygen can occur, causing the reduction of Mn^{4+} to Mn^{3+} [71]. As seen from the UV spectra, the Co^{2+} component decreased significantly in both types of catalysts, suggesting a reaction between Mn^{3+} and Co^{2+} (formed during calcination) with the consequent formation of the Mn_x-$Co_{3-x}O_4$ spinel (not detected in this work). However, the intensity of the Co^{2+} band (490–500 nm) was lower in the case of Co/SiO_2-0.7 catalyst, probably because its low specific surface area promoted more contact between Co and Mn particles. This finding is in accordance with the results of Raman spectroscopy characterization, where a lower intensity of the bands corresponding to Co_3O_4 was observed, suggesting an early "reduction" of Co oxide when the Mn content increased in the support. Similar results were observed on Co oxide by the addition of phosphorous to Co/TiO_2 catalyst [69].

It has been suggested that formation of solid solutions between Mn and Co could be favorable only at Mn/Co > 0.1, whereas at low ratios, only spinel is expected [22]. The formation of either the solid solution or the spinel in the boundary of the deposited Co oxide could contribute to the dissemination of the oxide particles, thus producing smaller particles [24]. From the UV–vis, Raman, and TPR results, it was found that the presence of Mn in the supports decreased the Co-oxide signals. This effect can be envisioned as a "wetting-like" effect of cobalt oxide over the supports, which is caused by the presence of Mn, resulting in Mn-Co spinel formation. These results are in agreement with those reported by Noronha et al. [63], who found with their Co/Nb_2O_5 catalyst that the Co^{2+} interacting with the support showed a lower reducibility besides being reduced at high temperature.

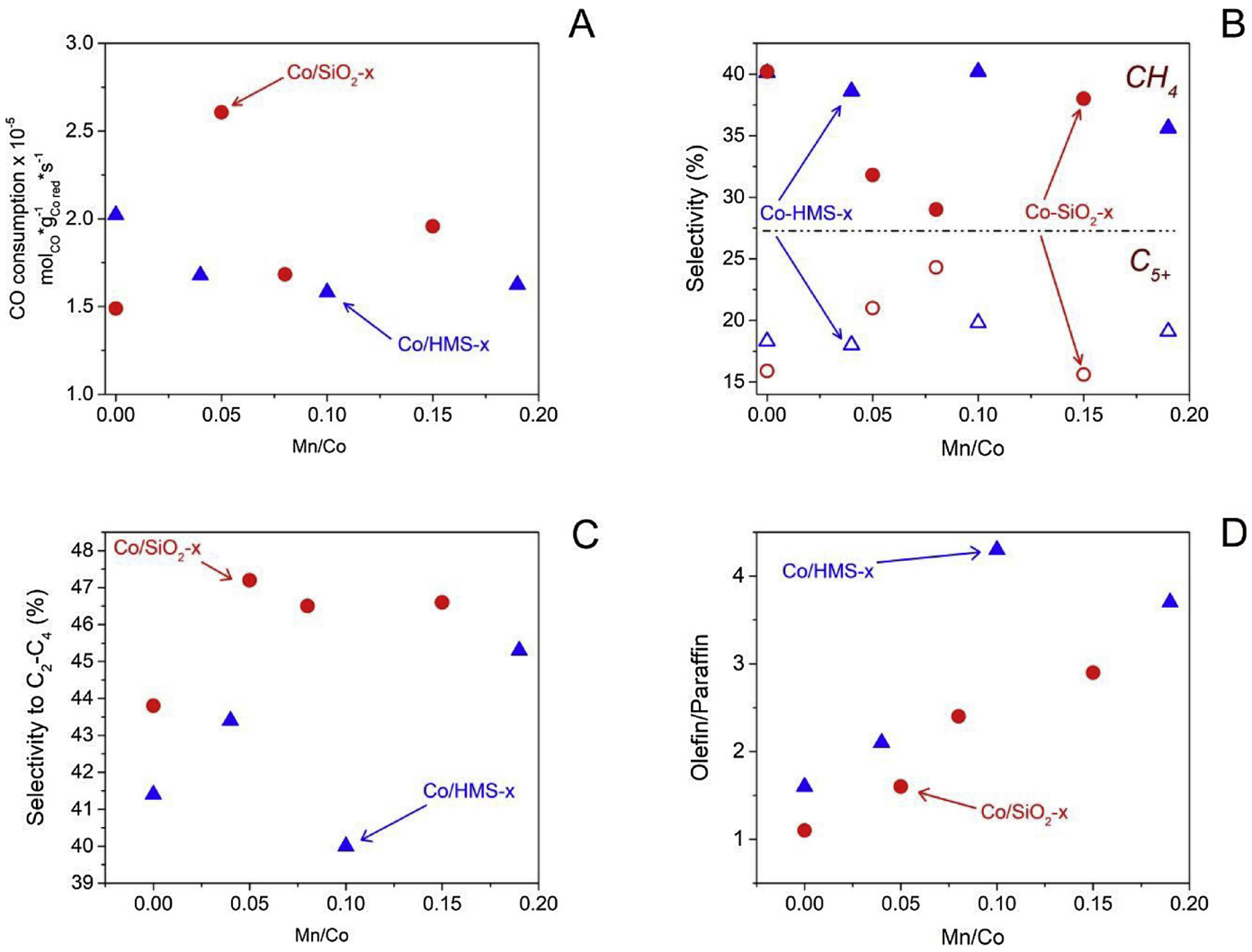

Fig. 10. Reaction results for the FTS reaction at atmospheric pressure for Co/SiO_2-x (●) and Co/HMS-x (▲) catalysts: (A) CO consumption rate, (B) Selectivity to CH_4 and C_{5+}, (C) Selectivity to C_2-C_4 hydrocarbons (olefin and paraffin compounds), and (D) Olefin/Paraffin ratio. Space Velocity = 21 nL/h*g_{cat}.

3.8. Catalytic activity and selectivity

Some authors [24,42,72,73] have reported that the catalytic activity and selectivity toward C_{5+} hydrocarbons decreased when the Co_3O_4 crystallite size is reduced to 10 nm. For the studied catalysts, it was not possible to address the influence of the crystallite size on the catalytic activity because the changes were not significant (from 13 to 10 nm in the absence of and with the highest Mn content, respectively); thus the Mn-Co interactions seem to be the main reason for the observed differences in the catalytic activity of both types of catalysts.

In Fig. 10A, the CO consumption rates at 220 °C and atmospheric pressure for the FTS reaction using the Co/SiO_2-*x* and Co/HMS-*x* catalysts are shown. The CO consumption rate was normalized by the amount of Co reduced at T ≤ 500 °C (see Eq. 1 and Table 3). Furthermore, the Mn/Co ratio (see Table 1) instead of the wt. % of Mn is used because the relationship between the reaction data and this ratio results in the best visualization.

As seen in Fig. 10A, both Co/HMS-*x* and Co/SiO_2-x catalysts showed essentially the same magnitude of the CO consumption rate despite their difference in surface areas, which indicates that the catalytic activity observed is related fundamentally with the Co loading in the catalysts. Additionally, it can be seen that the presence of Mn affected in a different manner the catalytic performance of the two types of catalysts. In the case of Co/SiO_2-x catalysts a small increase in the CO consumption was observed as function of the Mn loading, while for Co/HMS-x its presence was detrimental. On the other hand, the idea that Co particles are more segregated in the Co/HMS-x catalysts can explain the higher selectivity toward methane observed in the catalytic tests at low Mn loadings (Mn/Co < 0.1) (see Fig. 10B), and the slightly higher selectivity toward C_{5+} hydrocarbons compared with Co/SiO_2-*x* catalysts (Fig. 10B), which could be related to the effect of the HMS structure [14,15]. It has to be noted that the particle size obtained in both types of catalysts is close to those that are reported as highly selective for CH_4 formation [74]. Furthermore, the lower selectivity toward C_2-C_4 hydrocarbons showed by Co/HMS-x catalysts (Fig. 10C) and the slightly higher olefin to paraffin ratios at higher Mn contents (Fig. 10D) could be rationalized by the presence of dispersed and smaller particles that do not allow a large polymerization of adsorbed CO. It is proposed that the effect of Mn is to promote a higher retention of CO molecules on the active cobalt sites [16], which has as a consequence an increase in the amount of CO available for the polymerization reaction that can develop larger hydrocarbon chains.

In Fig. 11 are shown the CO consumption rates at 20 bar for the FTS reaction using the pelletized Co/SiO_2-x and Co/HMS-x catalysts and the selectivity toward light hydrocarbons for comparison with Fig. 10; the CO consumption rate was normalized by the amount of Co reduced at T ≤ 500 °C. Only representative catalysts were tested in order to observe the effect of the Mn presence in the FTS reaction at high pressures.

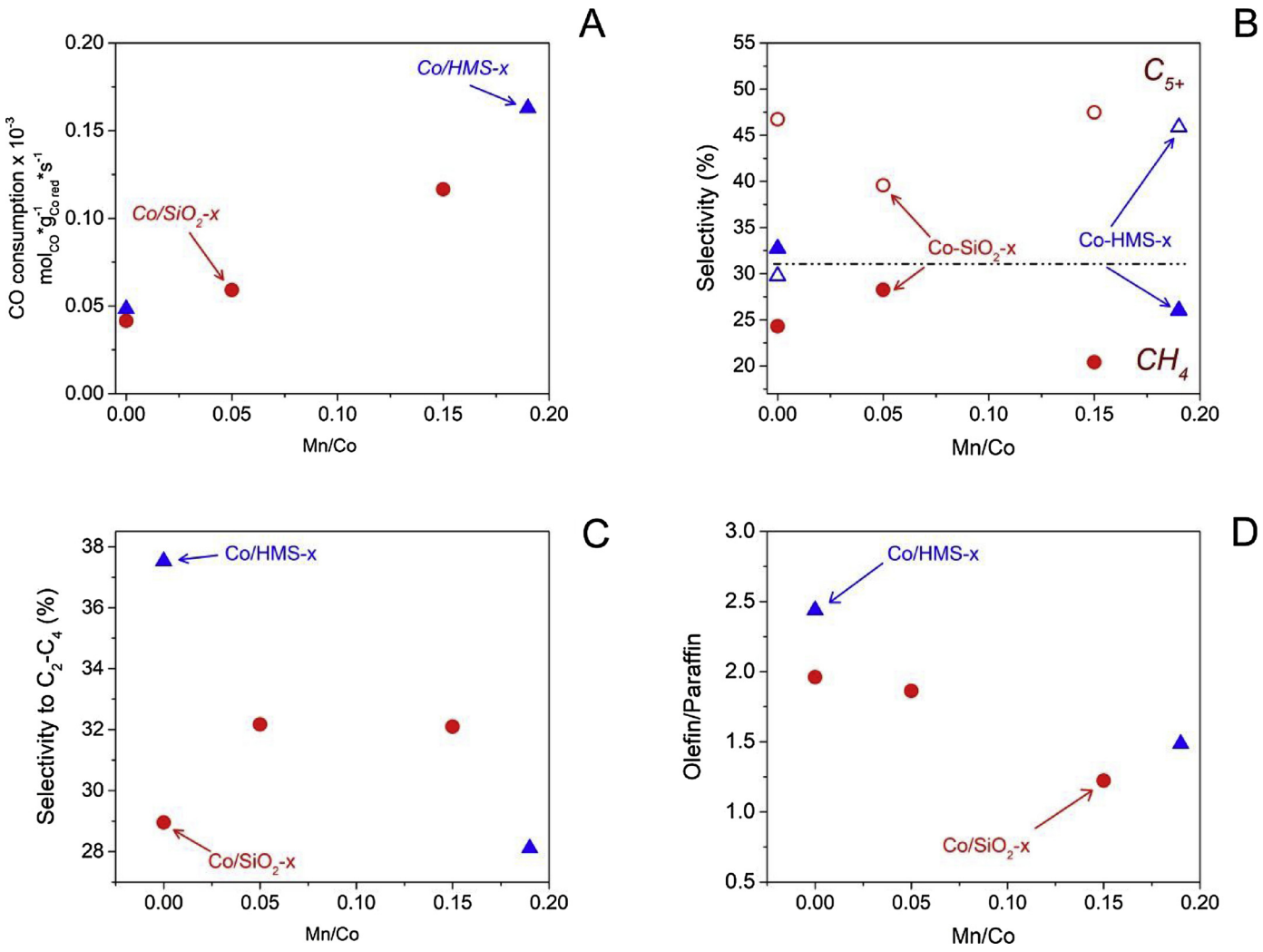

Fig. 11. Reaction results for the FTS reaction at 20 bar for Co/SiO_2-x (●) and Co/HMS-x (▲) catalysts: (A) CO consumption rate, (B) Selectivity to CH_4 and C_{5+}, (C) Selectivity to C_2-C_4 hydrocarbons (olefin and paraffin compounds), and (D) Olefin/Paraffin ratio. Space Velocity = 24 nL/h*g_{cat}.

As can be seen in Fig. 11A, for all catalysts there was an increase in the consumption rate of CO proportional to the Mn loading. The selectivity toward C_{5+} hydrocarbons was higher than at atmospheric pressure (Fig. 11B), the selectivity toward C_2-C_4 hydrocarbons for Co/HMS-0.19 catalyst showed an important decrease compared with Co/HMS (Fig. 11C) while the Co/SiO_2-x catalysts showed a similar behavior than at atmospheric pressure. The most remarkable is that at 20 bar the olefin/paraffin ratio is inverted respect to the observed behavior at atmospheric pressure with the increase in Mn content (Fig. 11D). This behavior in the O/P ratio is also seen for Fe-based catalysts at atmospheric pressure [75].

In Fig. 12 are shown the Time on Stream (TOS) curves and could be observed that the CO conversion for Co/HMS-x catalysts showed a little more stability compared with the Co/SiO_2-x catalysts, which could be in part caused because the control of temperature was not made inside the catalytic bed (see experimental section); the temperature in the catalytic bed ranged between 240–266 °C. However, the CO conversion was higher as the Mn loading increased, Both types of catalysts showed almost the same conversion with the highest Mn loading which suggests that the nature of the catalysts tends to be the same (because the HMS structure is not developed at high Mn contents). The last could explain why the distribution of the hydrocarbons in the wax composition tends to be virtually the same with the highest Mn loading (Fig. 13), whereas for the Mn-free catalysts, the Co/HMS catalyst showed a higher selectivity to heavier hydrocarbons.

The different selectivity observed for Co/SiO_2-x and Co/HMS-x catalysts indicates a marked contribution of the support in the hydrocarbon polymerization process. Table 5 shows the carbon balance where is observed that both types of catalysts were not fully selective toward hydrocarbons, suggesting that the production of oxygenated compounds and carbon dioxide (not measured in this work) is due to the presence of non-reduced Co-oxide species that are active for the water-gas shift, olefin isomerization, reinsertion, and hydrogenolysis [42]. Additionally, It can be observed that the presence of Mn in the Co-based catalysts leads to these behave as the Fe-based catalysts because the promotion of reactions that are observed in the latter [76,77].

The support´s texture has an important effect in the FTS reaction when the support has a small pore size (e.g., 4 nm) because capillary condensation, causing diffusion restrictions limiting the access of reactants to the catalysts though the gas-liquid interface [34]. It is expected that Co° particles are located outside of the HMS pores because the particles are larger (> 10 nm). Nevertheless the HMS have short channels that could communicate the Co° particles with the liquid wax condensed in the pores, thus the access of reactants to the active sites would be controlled by molecular diffusion in supports with narrow pore size if they are fully occupied with heavier hydrocarbons (liquid wax), such as it is expected for the case of Co-based catalysts, because to its high value of the chain growth probability factor (α) [73]. It is thought that this internal diffusional restriction could increase the contact time between the growing hydrocarbons and the active sites.

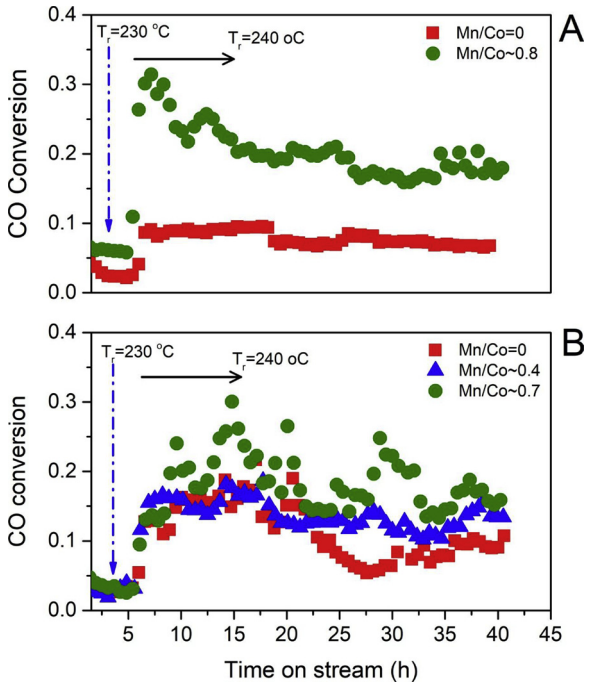

Fig. 12. CO conversion vs time on stream curves for Co/HMS-x (A) and Co/SiO_2-x (B). Reaction pressure = 20 bar, H_2/CO = 2, Space Velocity = 24 nL/h*g_{cat}.

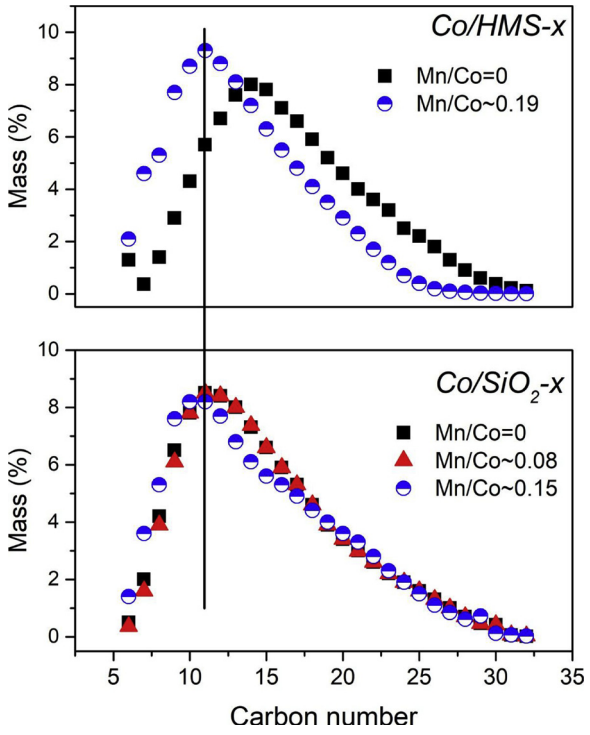

Fig. 13. Hydrocarbon compositions for liquid wax in the reaction tests at 20 bar (see Figs. 11 and 12), Co/HMS-x (A) and Co/SiO_2-x (B).

However if the catalyst has a low value of α, such as is the case of Fe-based catalysts, the pores will not completely filled with liquid wax. In these conditions the Knudsen diffusivity would have an important contribution, resulting in an increase of the effective diffusivity, promoting minor contact times because of the increase of mass transport.

On the other hand, it has been reported that the increase in the olefin to paraffin ratio could result from a higher Mn-Co interaction

Table 5
Reaction data for the catalytic tests at 20 bar, H_2/CO = 2, SV = 24 nL / h *g_{cat}.

Catalyst	CO conversion (%)	Consumption rate x 10^3 mole CO*$g_{Co\ reduced}^{-1}$*s^{-1}	O/P ratio	Carbon Balance (%)
Co/SiO_2	10	1.0	1.9	66
Co/SiO_2-0.4	12	1.5	1.8	64
Co/SiO_2-0.7	17	2.3	1.2	72
Co/HMS	6	1.1	2.5	65
Co/HMS-0.8	19	3.6	1.5	75

(e.g., [24]); this effect was seen at atmospheric pressure in both types of catalysts, mainly with the highest Mn loading (Fig. 10D), but at high pressure the opposite behavior was observed (Fig. 11D). Keyser et al. [78] found the same behavior when the FTS reaction was performed at high pressure on a Co/Mn oxide catalyst. They suggested that there are structural changes in the Co spinel that promote the increase of the hydrogenation activity as well as the WGS reaction.

Johnson et al. [74] reported that the maximum promotional effect on the FTS reaction when Mn is used as a promoter is found when it covers half of the Co surface, and it was found that this occurs at approximately Mn/Co ≈ 0.1. They proposed that the promotion is a consequence of Lewis acid-base interactions between the intermediate molecules of the reaction and the promoter cations. In this work, it was found that in the catalytic tests at atmospheric pressure, approximately at Mn/Co = 0.05, a good promotion effect of Mn is obtained for Co/SiO_2-x catalysts, which is in agreement with several authors and in contrast with the report by Johnson et al. [74]. Nevertheless, in the catalytic tests at 20 bar the CO consumption rate increases proportionally with the Mn loading for both Co/SiO_2-x and Co/HMS-x catalysts.

Finally, it can be seen that the explanation of Mn promotion on the catalysts is complex and has to be further investigated. There is a need to continue with investigations in order to understand the key aspects in the design of active and selective catalysts for the FTS reaction.

4. Conclusions

The low loadings of Mn used in this work hindered its characterization. However, its influence on the catalysts was observed from the characterization results, where it was observed that its presence in the supports promoted a “wetting-like” effect of the cobalt oxide on the surface of HMS-*x* and SiO_2-*x* (*x* = wt% of Mn) supports, leading to a small particle size of the cobalt oxide particles. This effect was observed from a decrease in the Raman and UV–vis signals of the only calcined catalysts and a minor reducibility of cobalt oxide as a result of the Co-Mn interactions (seen from TPR and XPS characterizations). It was found that Co^{2+} could be responsible for forming a spinel with the Mn deposited in the supports. On the other hand, the catalytic tests of the synthetized catalysts for the FTS reaction showed: i) at atmospheric pressure it was observed a slight improvement in the CO consumption rate and a slight increase in the chain growth of hydrocarbons at low Mn loadings, and ii) at 20 bar it was observed that CO consumption rate had a proportional increase with the Mn content in all tested catalyst, besides the selectivity toward light olefins was lower as the Mn content increased, suggesting the occurrence of secondary reactions such as WGS reaction, because the presence of Co-oxide species that were not reduced during the catalyst activation. Finally, these results suggest that cobalt sites in contact with Mn result in stable CO adsorption on the active sites that favored the polymerization reaction.

Acknowledgments

Hector G. Salazar gratefully acknowledges a graduate scholarship from CONACYT. This work was supported by grants from CONACYT

(Project No. 156064). The authors gratefully acknowledged the collaboration of Ricardo Rosas (I.Q.-UAM-I) for the XRD characterization and Miguel A. Gracia-Pinilla (FCFM-UANL) for the Raman characterization.

References

[1] World Shale Resource Assessments, U.S. Energy Information Administration, (2015) (Accessed 28 July 2018), https://www.eia.gov/analysis/studies/worldshalegas/.
[2] R. Lødeng, L. Hannevold, H. Bergem, M. Stöcker, K. Triantafyllidis, A. Lappas, M. Stöcker (Eds.), The Role of Catalysis for the Sustainable Production of Bio-fuels and Bio-chemicals, 1st ed., Elsevier B.V., 2013, pp. 351–396.
[3] G.W. Huber, S. Iborra, A. Corma, Chem. Rev. 106 (2006) 4044–4098.
[4] M.E. Dry, Catal. Today 71 (2002) 227–241.
[5] M. Nurunnabi, S.Q. Turn, Fuel Process. Technol. 130 (2015) 156–164.
[6] C. Kibby, K. Jothimurugesan, T. Das, H.S. Lacheen, T. Rea, R.J. Saxton, Catal. Today 215 (2013) 131–141.
[7] J.-S. Girardon, E. Quinet, A. Griboval-Constant, P.A. Chernavskii, L. Gengembre, A.Y. Khodakov, J. Catal. 248 (2007) 143–157.
[8] G.P. Van der Laan, A.A.C.M. Beenackers, Catal. Rev. Sci. Eng. 41 (1999) 255–318.
[9] D.J. Moodley, A.M. Saib, J. van de Loosdrecht, C.A. Welker-Nieuwoudt, B.H. Sigwebela, J.W. Niemantsverdriet, Catal. Today 171 (2011) 192–200.
[10] V. Meynen, P. Cool, E.F. Vansant, Microporous Mesoporous Mater. 125 (2009) 170–223.
[11] A. Tuel, Microporous Mesoporous Mater. 27 (1999) 151–169.
[12] T.R. Pauly, T.J. Pinnavaia, Chem. Mater. 13 (2001) 987–993.
[13] K. Cassiers, T. Linssen, M. Mathieu, M. Benjelloun, K. Schrijnemakers, P. Van Der Voort, P. Cool, E.F. Vansant, Chem. Mater. 14 (2002) 2317–2324.
[14] E. Lira, C.M. Lopez, F. Oropeza, M. Bartolini, J. Alvarez, M. Goldwasser, F.L. Linares, J.F. Lamonier, M.J.P. Zurita, J. Mol. Catal. A-Chem. 281 (2008) 146–153.
[15] L.F.F.P.G. Braganca, M. Ojeda, J.L.G. Fierro, M.I.P. da Silva, Appl. Catal. A-Gen. 423 (2012) 146–153.
[16] M. Jiang, N. Koizumi, T. Ozaki, M. Yamada, Appl. Catal. A-Gen. 209 (2001) 59–70.
[17] D.H. Yin, W.H. Li, W.S. Yang, H.W. Xiang, Y.H. Sun, B. Zhong, S.Y. Peng, Microporous Mesoporous Mater. 47 (2001) 15–24.
[18] A. Martinez, C. Lopez, F. Marquez, I. Diaz, J. Catal. 220 (2003) 486–499.
[19] T.E. Feltes, L. Espinosa-Alonso, E. de Smit, L. D'Souza, R.J. Meyer, B.M. Weckhuysen, J.R. Regalbuto, J. Catal. 270 (2010) 95–102.
[20] J.P. den Breejen, A.M. Frey, J. Yang, A. Holmen, M.M. van Schooneveld, F.M.F. de Groot, O. Stephan, J.H. Bitter, K.P. de Jong, Top. Catal. 54 (2011) 768–777.
[21] Y.P. Li, X.X. Qin, T.J. Wang, L.L. Ma, L.G. Chen, N. Tsubaki, Fuel 136 (2014) 130–135.
[22] A. Dinse, M. Aigner, M. Ulbrich, G.R. Johnson, A.T. Bell, J. Catal. 288 (2012) 104–114.
[23] G.R. Johnson, S. Werner, A.T. Bell, Am. Chem. Soc.: Catal. 5 (2015) 5888–5903.
[24] F. Morales, E. de Smit, F.M.F. de Groot, T. Visser, B.M. Weckhuysen, J. Catal. 246 (2007) 91–99.
[25] G. Prieto, M.I.S. De Mello, P. Concepción, R. Murciano, S.B.C. Pergher, A. Martínez, Am. Chem. Soc.: Catal. 5 (2015) 3323–3335.
[26] K. Guse, H. Papp, Fresen J. Anal. Chem. 346 (1993) 84–91.
[27] R. Malessa, M. Baerns, Ind. Eng. Chem. Res. 27 (1988) 279–283.
[28] T. Herranz, S. Rojas, F.J. Perez-Alonso, A. Ojeda, P. Terreros, J.L.G. Fierro, Appl. Catal. A-Gen. 311 (2006) 66–75.
[29] A. Campos, N. Lohitharn, A. Roy, E. Lotero, J.G. Goodwin, J.J. Spivey, Appl. Catal. A-Gen. 375 (2010) 12–16.
[30] N. Lohitharn, J.G. Goodwin, E. Lotero, J. Catal. 255 (2008) 104–113.
[31] M.C. Ribeiro, G. Jacobs, R. Pendyala, B.H. Davis, D.C. Cronauer, A.J. Kropf, C.L. Marshall, J. Phys. Chem. C 115 (2011) 4783–4792.
[32] J.D. Xu, K.T. Zhu, X.F. Weng, W.Z. Weng, C.J. Huang, H.L. Wan, Catal. Today 215 (2013) 86–94.
[33] B.H. Davis, Catal. Today 84 (2003) 83–98.
[34] P.T. Tanev, T.J. Pinnavaia, Chem. Mater. 8 (1996) 2068–2079.
[35] CasaXPS software, http://www.casaxps.com/, (Accessed 28 July 2018).
[36] P.A. Webb, C. Orr, Analytical Methods in Fine Particle Technology, (1997).
[37] D.F. Enache, E. Vasile, C.M. Simonescu, D. Culita, E. Vasile, O. Oprea, A.M. Pandele, A. Razvan, F. Dumitru, G. Nechifor, RSC Adv. 8 (2018) 176–189.
[38] W.B. Yue, W.Z. Zhou, J. Mater. Chem. 17 (2007) 4947–4952.
[39] F. Morales, D. Grandjean, A. Mens, F.M.F. de Groot, B.M. Weckhuysen, J. Phys. Chem. B 110 (2006) 8626–8639.
[40] H.F. Xiong, Y.H. Zhang, K.Y. Liew, J.L. Li, Fuel Process. Technol. 90 (2009) 237–246.
[41] O. Gonzalez, H. Perez, P. Navarro, L.C. Almeida, J.G. Pacheco, M. Montes, Catal. Today 148 (2009) 140–147.
[42] A.Y. Khodakov, W. Chu, P. Fongarland, Chem. Rev. 107 (2007) 1692–1744.
[43] A.Y. Khodakov, J. Lynch, D. Bazin, B. Rebours, N. Zanier, B. Moisson, P. Chaumette, J. Catal. 168 (1997) 16–25.
[44] D.G. Klissurski, E.L. Uzunova, Appl. Surf. Sci. 214 (2003) 370–374.
[45] F. Morales, F.M.F. de Groot, P. Glatzel, E. Kleimenov, H. Bluhm, M. Hävecker, A. Knop-Gericke, B.M. Weckhuysen, J. Phys. Chem. B 108 (2004) 16201–16207.
[46] B.H. Davis, Catal. Today 141 (2009) 25–33.
[47] B. Ernst, S. Libs, P. Chaumette, A. Kiennemann, Appl. Catal. A-Gen. 186 (1999) 145–168.
[48] N. Das, H. Eckert, H. Hu, I.E. Wachs, J.F. Walzer, F.J. Feher, J. Phys. Chem. 97 (1993) 8240–8243.
[49] Z. Luan, P.A. Meloni, R.S. Czernuszewicz, L. Kevan, J. Phys. Chem. B 101 (1997) 9046–9051.
[50] T.A. Zepeda, A. Infantes-Molina, J.N. Díaz de Leon, R. Obeso-Estrella, S. Fuentes, G. Alonso-Nuñez, B. Pawelec, J. Mol. Catal. A Chem. 397 (2015) 26–35.
[51] J. Gnado, P. Dhamelincourt, C. Pelegris, M. Traisnel, A.L. Mayot, J. Non-Cryst. Solids 208 (1996) 247–258.
[52] C.-B. Wang, C.-C. Lee, J.-L. Bi, J.-Y. Siang, J.-Y. Liu, C.-T. Yeh, Catal. Today 146 (2009) 76.
[53] C.-W. Tang, C.-B. Wang, S.-H. Chien, Thermochim. Acta 473 (2008) 68–73.
[54] P. Rybak, B. Tomaszewska, A. Machocki, W. Grzegorczyk, A. Denis, Catal. Today 176 (2011) 14–20.
[55] F. Buciuman, F. Patcas, R. Craciun, D.R.T. Zahn, Phys. Chem. Chem. Phys. 1 (1999) 185–190.
[56] J. Xu, Y.-Q. Deng, X.-M. Zhang, Y. Luo, W. Mao, X.-J. Yang, L. Ouyang, P. Tian, Y.-F. Han, ACS Catal. 4 (2014) 4106–4115.
[57] S.G. Aspromonte, A. Sastre, A.V. Boix, M.J. Cocero, E. Alonso, Microporous Mesoporous Mater. 148 (2012) 53–61.
[58] S.H. Liang, F.T.G. Bulgan, R.L. Zong, Y.F. Zhu, J. Phys. Chem. C 112 (2008) 5307–5315.
[59] K. Ramesh, L.W. Chen, F.X. Chen, Y. Liu, Z. Wang, Y.F. Han, Catal. Today 131 (2008) 477–482.
[60] L. Frunza, J. Pelgrims, H. Leeman, P. Van Der Voort, E.F. Vansant, R.A. Schoonheydt, B.M. Weckhuysen, J. Phys. Chem. B 105 (2001) 2677–2686.
[61] B.J. Aronson, C.F. Blanford, A. Stein, J. Phys. Chem. B 104 (2000) 449–459.
[62] B. Solsona, T.E. Davies, T. Garcia, I. Vazquez, A. Dejoz, S.H. Taylor, Appl. Catal. B-Environ. 84 (2008) 176–184.
[63] F.B. Noronha, C.A. Perez, M. Schmal, R. Frety, Phys. Chem. Chem. Phys. 1 (1999) 2861–2867.
[64] W.A. Carvalho, P.B. Varaldo, M. Wallau, U. Schuchardt, Zeolites 18 (1997) 408–416.
[65] J. Taghavimoghaddam, G.P. Knowles, A.L. Chaffee, J. Mol. Catal. A-Chem. 358 (2012) 79–88.
[66] S. Farhadi, M. Javanmard, G. Nadri, Acta Chim. Slov. 63 (2016) 335–343.
[67] A.P. Katsoulidis, D.E. Petrakis, G.S. Armatas, P.N. Trikalitis, P.J. Pomonis, Microporous Mesoporous Mater. 92 (2006) 71–80.
[68] L.G.A. van de Water, G.L. Bezerner, J.A. Bergwerff, M. Versluijs-Helder, B.M. Weckhuysen, K.P. de Jong, J. Catal. 242 (2006) 287–298.
[69] Y. Brik, M. Kacimi, M. Ziyad, F. Bozon-Verduraz, J. Catal. 202 (2001) 118–128.
[70] Z.W. Chen, Z. Jiao, D.Y. Pan, Z. Li, M.H. Wu, C.H. Shek, C.M.L. Wu, J.K.L. Lai, Chem. Rev. 112 (2012) 3833–3855.
[71] E. Vila, R.M. Rojas, J.L.M. de Vidales, O. Garcia-Martinez, Chem. Mater. 8 (1996) 1078–1083.
[72] N. Fischer, E. van Steen, M. Claeys, J. Catal. 299 (2013) 67–80.
[73] G. Prieto, A. Martínez, P. Concepción, R. Moreno-Tost, J. Catal. 266 (2009) 129–144.
[74] G.R. Johnson, A.T. Bell, J. Catal. 338 (2016) 250–264.
[75] J.R.G. Sánchez-López, A. Martínez-Hernández, A. Hernandez-Ramírez, Rev. Chem. Eng. 33 (2016) 109–142.
[76] F. Morales, B.M. Weckhuysen, Catalysis (R. Soc. Chem.) 19 (2006) 1–40.
[77] M.J. Keyser, R.-C. Everson, R.L. Espinoza, Ind. Eng. Chem. Res. 39 (2000) 48–54.
[78] M.J. Keyser, R.C. Everson, R.L. Espinoza, Appl. Catal. A-Gen. 171 (1998) 99–107.